ASTRONOMY
AND
ASTROPHYSICS

Rotation and chromospheric activity in field M dwarfs[*]

X. Delfosse[1], **T. Forveille**[1], **C. Perrier**[1], **and M. Mayor**[2]

[1] Observatoire de Grenoble, 414 rue de la Piscine, Domaine Universitaire de St Martin d'Hères, F-38041 Grenoble, France
[2] Observatoire de Genève, CH-1290 Sauverny, Switzerland

Abstract. We have obtained high resolution spectra for a volume-limited sample of 118 field M dwarfs. From these observations we derive projected rotational velocities and fluxes in the H_α and H_β lines[1]. 8 stars are double-lined spectroscopic binaries with measured or probable periods short enough for rotation to be tidally synchronized with the orbit, and another 11 are visual binaries where we cannot yet separate the lines of the two stars. Of the remaining 99 stars, 24 have rotational velocities above our detection limit of ~ 2 km.s^{-1}, and some are quite fast rotators, including two with v sin $i \simeq 30$ km.s^{-1} and one with v sin $i \simeq 50$ km.s^{-1}. Given the small radii of M dwarfs, these moderate rotational velocities correspond to rather short maximum rotational periods, of only 7-8 hours. These three stars are good candidates for Doppler imaging.

We find that rotation is strongly correlated with both spectral type and kinematic population: all stars with measurable rotation are later than M3.5, and all but one have kinematic properties typical of the young disk, or intermediate between the young disk and the the old disk. We interpret this correlation as evidence for a spin-down timescale that increases with decreasing mass. At the age of the old disk or halo, all stars earlier than M5-M6 (0.1-0.15M$_\odot$) have spun-down to below our detection limit, while at the age of the young disk this has only happened for stars earlier than M3.5. The one star with measurable rotation and a kinematics intermediate between old disk and population II has spectral type M6. It is probably an old star whose mass is low enough that it has retained significant rotation up to present, still consistently with longer spin-down times for lower mass stars. We observe, on the other hand, no conspicuous change in the v sin i distribution or activity pattern at the mass (M~ 0.35 $M_\odot$) below which stars remain fully convective down to the main sequence.

These new data are consistent with a saturated correlation between rotation and activity, similar to the one observed for younger or more massive stars: L_X/L_{bol} and L_{H_α}/L_{bol} both correlate with v sin i for v sin $i \lesssim 4-5$ km.s^{-1} and then saturate at respectively $10^{-2.5}$ and $10^{-3.5}$.

Key words: stars: activity – stars: rotation – stars: chromospheres – stars: coronae – stars: low-mass, brown dwarfs

1. Introduction

Surface rotation is a key observational parameter for stellar evolution, as a diagnostic of the mechanisms responsible for stellar angular momentum loss and internal angular momentum transport. The latter are responsible for chemical mixing and they modify the stellar thermal structure (e.g. Martin & Claret 1996), and hence affect the overall evolution. Rotation is also the driving force behind stellar activity (coronae, chromospheres, spots, flares), through dynamo production of magnetic fields.

Pre-main-sequence rotational evolution of low mass stars is generaly presumed to be dominated by magnetic coupling with the parent protostellar disk (Cameron & Campbell 1993, Shu et al. 1994): as long as a star is surrounded by a substantial accretion disk, its equatorial velocity remains approximately constant at ~ 20 km.s^{-1} (e.g. Bouvier et al. 1993). Once accretion stops, disk braking disappears, and angular momentum conservation then becomes the dominant factor. Stars therefore spin up during their contraction along an Hayashi track, as their moment of inertia decreases. Since the time at which this happens depends on details of their circumstellar environment, stars arrive on the ZAMS with a broad distribution of rotational velocities (e.g. Bouvier et al. 1997). Once on the main sequence the moment of inertia no longer changes significantly. As first suggested by Schatzman (1962), magnetic winds then brake down the stars to low final equatorial velocities, approximately with a $t^{-1/2}$ Skumanich (1972) law. The time scale for this angular momentum dissipation is mass-dependent: rapid rotators are found at all spectral types (G-M) at the age of the α Persei cluster (~ 50 Myr) (Prosser 1991), in the Pleiades (~ 70 Myr) only later than mid-K (Stauffer & Hartmann, 1987), and in the Hyades (~ 600

Myr) only within the M dwarfs (Stauffer et al. 1987; Stauffer et al. 1997). The situation in the field is slightly less clear, since several age groups are represented, but all G dwarfs rotate slowly, and there are good spectroscopic or dynamic arguments to attribute a (very) young age to all K-early M rapid rotators.

Over the years, a large observational effort has established this picture of rotation along low mass stellar tracks, and models incorporating the above general elements (e.g. Bouvier & Forestini 1995, Krishnamurthi et al. 1997) successfully reproduce the rotational velocity distribution of solar mass dwarfs at all ages: pre-main-sequence T Tauri and post-T Tauri star, young main sequence stars in open clusters, and field stars.

Some aspects of the models however remain largely phenomenological, mostly because the complex physics of accretion and stellar dynamos is only partly understood. A number of competing models therefore exist, that differ on, for instance, radiative core/convective envelope decoupling, or parameterisation of the angular momentum loss law. The uncertain physical mechanisms are expected to have a strong mass dependence, and it is therefore useful to extend the observational database to the lower mass M dwarfs (e.g. Krishnamurthi et al. 1997). The [M0V,M6V] range is also interesting because it contains the mass ($\sim0.35\ M_\odot$, M2.5V) below which main sequence stars no longer develop a radiative core. The radiative/convective boundary layer is essential (e.g. Spiegel & Weiss 1980; Spruit & van Ballegooijen 1982) to the operation of the standard $\alpha - \Omega$ shell dynamo which is generally believed to generate the large scale solar magnetic field, and a break in both the activity level and the rotation properties could, at least naively, be expected at this spectral type.

A number of authors have discussed the rotation behaviour of M dwarfs in young open clusters (most recently Stauffer et al. (1997) for the Hyades, Stauffer et al. (1994) for the Pleiades, Patten & Simon (1996) for IC 2391), but there are fewer studies for field M dwarfs. Stauffer & Hartmann (1986) measured v sin i for approximately 200 field M dwarfs with a $10\,\mathrm{km.s}^{-1}$ sensitivity. Only 11 have significant broadening, a few of which may actually be unrecognized double-lined spectroscopic binaries. Marcy & Chen (1992) observed 47 field M dwarfs with v sin i sensitivity of $\sim3\,\mathrm{km.s}^{-1}$, only five of which have detectable rotation, all with v sin $i < 10\,\mathrm{km.s}^{-1}$. Both surveys have relatively bright limiting magnitudes (V=12 and V=11, respectively) and as a consequence preferentially sample early M dwarfs. More recently, two papers have examined the rotation of very low mass field stars (M6 or later). Martin et al. (1996) have determined rotational periods for a set of very late (M6-M9) dwarfs, and all 6 field stars in their sample have very short rotational periods <8 hours ($V_{eq} > 20\,\mathrm{km.s}^{-1}$). Basri & Marcy (1995) have measured v sin i for 5 extreme cool field dwarfs, of which 3 rotate, including the brown dwarf candidate BRI 0021-0214 (M9.5+, v sin i =40 $\mathrm{km.s}^{-1}$). Surprisingly, BRI 0021-0214 is a rapid rotator but has very weak (Basri & Marcy 1995) though detectable (Tinney et al. 1997) chromospheric activity, as measured by H_α emission. This suggests a possible change in the rotation/activity relation for the latest M dwarfs, and it is therefore important to examine slightly earlier M dwarfs.

Table 1. Stars with $d \leq 9pc$ and $\delta \geq -16°$ too faint to be measured with ELODIE

name	α (2000.)	δ (2000.)	spectral type	m_V
LHS 1326	02:02:16.1	+10:20:17	M6	15.61
LHS 1375	02:16:29.8	+13:35:17	M5.5	15.79
Gl 105C	02:35:58.7	+06:52:00	$\geq$M7	$\geq$ 16
LHS 2065	08:53:36.3	−03:29:33	M9	18.8
LHS 292	10:48:12.7	−11:20:13	M6.5	15.6
Gl 644C(VB8)	16:55:34.9	−08:23:43	M7	16.7
Gl 752B(VB10)	19:16:57.5	+05:09:02	M8	17.5

In the course of a radial velocity survey for low mass companions and planets around nearby M dwarfs (Delfosse et al. 1997), we have obtained high resolution optical spectra for a volume-limited sample of 118 K5 to M6.5 dwarfs. Here we analyse the accurate v sin i measurements (or significant upper limits, $\lesssim 2\,\mathrm{km.s}^{-1}$) that we derive from those data, using digital correlation techniques. They fill the spectral type gap between the generally earlier slow rotators measured by Marcy & Chen (1992) and the later than M6 very low mass rapid rotators observed by Basri & Marcy (1995) and Martin et al. (1996). This brings important new constraints on angular momentum dissipation in mid-M dwarfs at a few Gyr.

2. Observations and data processing

2.1. Sample selection

As we are interested in a fair sampling of M spectral subtypes, we decided to observe a volume-limited sample and initially selected all M dwarfs in the third edition of the nearby star catalog (Gliese and Jahreiss 1991) with a distance closer than 9 pc and a declination above -16 degrees. 136 stars fullfill these criteria. Of these, 7 (listed in Table 1) have apparent magnitudes fainter than V=15 and had to be dropped because they are beyond the sensitivity limit of the instrument we used. Gl 53B and Gl 451B are close companions to the much brighter Gl 53A (G5 VI) and Gl 451A (G8 VI) from which they cannot be separated by the spectrograph input fiber, and they were thus not observed. 7 very close pairs (<1") have two separate entries in the Gliese catalog but had to be merged for this program, and two slightly wider binaries (GJ 1103AB and GJ 1116AB) could not be separated under the seeing conditions that prevailed when they were observed and only have a joint spectrum for the pair. We therefore have obtained spectra for 118 stars or systems.

2.2. Instrumental setup

All observations were obtained at Observatoire de Haute Provence with the ELODIE spectrograph (Baranne et al. 1996) on the 1.93m telescope, between September 1995 and March 1997. This fixed configuration dual-fiber-fed echelle spectrograph covers in a single exposure the 390-680 nm spectral range, at an average resolving power of 42000. Elaborate online processing is integrated with the spectrograph control software, and automatically produces optimally extracted and wave-

Table 2. Basic parameters of the sample stars, which have been selected from the CNS3 (Gliese & Jahreiss 1991) as having d<9pc and $\delta > -16$ deg. Spectral type are from Reid et al (1995a), except [a] from Henry et al. (1994). $(R-I)_c$ is from Leggett's (1992) compilation, except: [b] from the CNS3 catalog (Gliese and Jahreiss, 1991; the Kron R-I in the CNS3 were transformed to the Cousins system using the Bessel (1983) relation, $(R-I)_c = 1.20(R-I)_K + 0.08$; [c] from Bessel (1990); [d] estimated from spectral type, using Leggett's (1992) relation for the Young Disk. Parallax and proper motion are from [e] the Yale General Catalogue of Trigonometric Stellar Parallaxes (Van Altena et al. 1991), or [f] the Hipparcos input catalogue (Turon et al 1993).

Name	α (J2000.0)	δ (J2000.0)	spectral type	$(R-I)_c$	M_V	M_{BOL}	parallax (mas)	err. par.	pmRA (".yr^{-1})	pmDec (".yr^{-1})	V_r (km.s^{-1})
GJ 1002	00:06:42.7	−07:32:44.5	M5.5	2.00	15.39	11.72	213[e]	3	−0.820	−1.887	−41
Gl 15A	00:18:23.3	+44:01:23.7	M1	1.14[b]	10.30	8.81	278[f]	7	2.885	0.419	11
Gl 15B	00:18:25.5	+44:01:44.2	M3.5	1.58	13.30	10.82	281[e]	3	2.886	0.373	11
Gl 34B	00:49:05.8	+57:48:57.4	K7[a]	0.80[b]	8.66	7.77	170[e]	2	1.099	−0.526	11
Gl 48	01:02:32.2	+71:40:47.1	M3	1.38[b]	10.25	8.24	110[f]	5	1.715	−0.408	1
Gl 49	01:02:38.8	+62:20:41.8	M1.5	1.15[b]	9.69	8.17	106[f]	9	0.683	0.064	−6
LP 467−16	01:11:25.8	+15:26:19.6	M5	1.94[b]	14.72	11.23	118[e]	21	0.176	−0.123	4
Gl 70	01:43:20.2	+04:19:18.0	M2	1.27[c]	11.18	9.41	112[f]	14	−0.422	−0.753	−26
Gl 83.1	02:00:13.1	+13:02:55.7	M4.5	1.75	14.02	11.08	223[e]	3	1.084	−1.777	−29
Gl 105B	02:36:16.8	+06:52:26.2	M4	1.60	12.30	9.76	134[e]	2	1.800	1.467	26
Gl 109	02:44:15.5	+25:31:24.0	M3	1.38[b]	11.14	9.14	130[f]	8	0.843	−0.379	30
GJ 1057	03:13:22.5	+04:46:27.8	M5	1.85	14.14	10.92	117[e]	4	1.737	0.103	27
Gl 166C	04:15:21.7	−07:39:28.8	M4.5	1.63	12.74	10.12	206[e]	2	−2.239	−3.409	−45
Gl 169.1A	04:31:11.8	+58:58:38.1	M4	1.60	12.33	9.79	178[f]	2	1.273	−2.052	28
LHS 1723	05:01:57.0	−06:56:47.1	M4	1.68[b]	13.16	10.41	163[e]	26	−0.546	−0.548	42
Gl 205	05:31:27.3	−03:40:39.1	M1.5	1.10	9.02	7.61	163[f]	5	0.755	−2.103	8
Gl 213	05:42:09.3	+12:29:21.1	M4	1.61	12.58	10.01	162[f]	4	2.008	−1.607	105
LHS 1805	06:01:09.7	+59:35:41.8	M3.5	1.53[b]	12.31	9.95	132[e]	3	−0.108	0.917	1
G 099−049	06:00:05.3	+02:42:19.6	M4	1.60[d]	12.68	10.14	186[e]	7	0.299	−0.023	30
Gl 232	06:24:41.6	+23:25:53.1	M4.5	1.64	13.46	10.81	120[e]	2	0.390	−0.300	−12
Gl 234AB	06:29:23.4	−02:48:50.8	M4.5	1.71	13.10	10.27	248[f]	4	0.708	−0.706	15
Gl 251	06:54:48.9	+33:16:05.6	M3	1.41	11.16	9.09	170[f]	4	−0.756	−0.390	22
LHS 1885	06:57:57.9	+62:19:09.2	M4.5	1.84[b]	14.20	11.01	129[e]	20	0.332	−0.395	16
GJ 1093	06:59:28.4	+19:20:40.0	M5	1.90[b]	15.38	12.02	129[e]	4	0.908	−0.889	−30
Gl 268.3AB	07:16:19.8	+27:08:31.9	M2.5	1.43[b]	11.35	9.23	126[f]	25	−0.036	−0.266	−6
Gl 273	07:27:24.5	+05:13:32.5	M3.5	1.55	11.97	9.56	266[f]	3	0.573	−3.716	18
G 089−032	07:36:25.3	+07:04:34.4	M5	1.86[b]	14.27	11.02	162[e]	26	0.265	−0.351	24
Gl 285	07:44:40.1	+03:33:08.7	M4.5	1.69	12.26	9.49	163[f]	4	−0.399	−0.449	26
GJ 1105	07:58:12.8	+41:18:13.3	M3.5	1.53[b]	12.43	10.07	122[f]	3	0.215	−0.678	−21
Gl 299	08:11:57.4	+08:46:27.4	M4.5	1.67	13.68	10.96	148[e]	3	1.210	−5.260	14
GJ 2066	08:16:07.9	+01:18:09.1	M2	1.23[b]	10.37	8.69	113[f]	4	−0.414	0.055	62
GJ 1111	08:29:48.5	+26:46:31.7	M6	2.26	17.01	12.50	276[e]	3	−1.110	−0.603	9
GJ 2069B	08:31:37.6	+19:23:55.3	M4	1.71[b]	13.60	10.78	114[e]	13	−0.256	−0.113	4
Gl 338A	09:14:22.7	+52:41:11.5	K7	0.90[b]	8.65	7.60	161[f]	4	−1.568	−0.612	11
Gl 338B	09:14:24.7	+52:41:11.0	K7	0.91[b]	8.74	7.67	161[f]	4	−1.568	−0.612	12
Gl 380	10:11:22.2	+49:27:14.7	K5	0.77	8.32	7.47	222[f]	5	−1.343	−0.519	−26
Gl 382	10:12:17.7	−03:44:43.7	M1.5	1.18	9.61	8.04	117[f]	5	−0.154	−0.228	7
Gl 388	10:19:36.3	+19:52:11.5	M3	1.42	10.95	8.85	204[e]	2	−0.503	−0.054	12
Gl 393	10:28:55.6	+00:50:27.0	M2	1.23	10.18	8.50	128[f]	8	−0.585	−0.741	8
Gl 402	10:50:52.1	+06:48:29.5	M4	1.58	12.35	9.86	138[f]	6	−0.816	−0.807	−2
Gl 406	10:56:29.2	+07:00:47.6	M5.5	2.18	16.56	12.32	419[e]	2	−3.830	−2.680	16
Gl 408	11:00:04.3	+22:49:59.4	M2.5	1.34	10.89	8.97	149[f]	8	−0.403	−0.228	3
Gl 411	11:03:20.2	+35:58:11.2	M2	1.14	10.45	8.95	392[f]	4	−0.575	−4.767	−85
Gl 412A	11:05:28.5	+43:31:37.0	M0.5	1.02	9.93	8.66	173[f]	10	−4.424	0.955	68
Gl 412B	11:05:30.9	+43:31:16.1	M6	2.10	15.59	11.61	173[e]	10	−4.424	0.955	68
Gl 424	11:20:04.8	+65:50:47.7	M0	0.98	9.67	8.48	118[f]	7	−2.953	0.191	60
Gl 445	11:47:41.3	+78:41:28.5	M3.5	1.52	12.26	9.92	196[f]	8	0.712	−0.492	−112
Gl 447	11:47:44.4	+00:48:17.0	M4	1.68	13.49	10.74	298[f]	5	0.635	−1.186	−31

Table 2. (continued)

Name	α (J2000.0)	δ (J2000.0)	spectral type	$(R-I)_c$	M_V	M_{BOL}	parallax (mas)	err. par.	pmRA (".yr^{-1})	pmDec (".yr^{-1})	V_r (km.s^{-1})
GJ 1151	11:50:58.4	+48:22:35.9	M4.5	1.74^b	13.66	10.75	121^e	3	−1.518	−0.948	−37
Gl 450	11:51:07.3	+35:16:19.4	M1	1.14	9.90	8.40	108^f	5	−0.298	0.275	0
LHS 2520	12:10:05.2	−15:04:17.4	M3.5	1.57^b	12.31	9.84	112^e	21	−0.050	−0.718	80
GJ 1154A	12:14:15.6	+00:37:45.8	M5	1.78^b	14.11	11.09	119^e	3	−0.934	−0.285	−14
GJ 1156	12:18:59.5	+11:07:31.5	M5	1.99^b	14.73	11.10	153^e	3	−1.243	0.216	4
Gl 486	12:47:56.6	+09:45:05.5	M3.5	1.55	11.53	9.12	107^f	12	−0.988	−0.421	18
Gl 493.1	13:00:32.8	+05:41:09.1	M4.5	1.76^c	13.85	10.88	123^e	4	−0.913	0.232	−27
GJ 2097	13:07:02.3	+20:48:56.9	M1.5	1.74^b	13.55	10.64	156^e	23	−0.069	−0.038	−12
Gl 514	13:29:59.7	+10:22:37.5	M0.5	1.05	9.46	8.14	121^f	11	1.113	−1.079	14
G 165−08	13:31:46.3	+29:16:29.4	M4	1.59	12.45	9.94	126^e	22	−0.245	−0.114	8
Gl 526	13:45:43.8	+14:53:27.8	M1.5	1.08	9.99	8.61	202^f	4	1.791	−1.479	15
Gl 555	14:34:16.8	−12:31:10.2	M4	1.62	12.20	9.61	151^f	7	−0.343	0.602	−2
Gl 581	15:19:26.9	−07:43:23.1	M3	1.41	11.43	9.35	149^f	5	−1.184	−0.296	−10
Gl 623	16:24:09.3	+48:21:10.6	M2.5	1.31	10.88	9.03	132^f	7	1.154	−0.443	−27
Gl 625	16:25:24.7	+54:18:15.3	M1.5	1.22	11.03	9.37	152^f	2	0.455	−0.139	−13
Gl 628	16:30:18.1	−12:39:45.2	M3.5	1.51	12.02	9.70	244^f	6	−0.053	−1.169	−22
Gl 643	16:55:25.4	−08:19:19.4	M3.5	1.54	12.87	10.49	164^f	5	−0.800	−0.881	15
Gl 673	17:25:45.3	+02:06:41.1	K5	0.76	8.03	7.19	126^f	4	−0.571	−1.183	−24
Gl 686	17:37:53.4	+18:35:31.0	M1	1.12	10.19	8.74	130^f	3	0.927	0.998	−10
Gl 687	17:36:26.0	+68:20:21.5	M3	1.41	10.73	8.65	204^f	4	−0.316	−1.258	−29
Gl 699	17:57:48.5	+04:41:35.8	M4	1.57	13.23	10.77	545^f	3	−0.803	10.278	−111
Gl 701	18:05:07.5	−03:01:52.4	M1	1.08	10.00	8.62	133^f	6	0.555	−0.330	32
GJ 1224	18:07:32.9	−15:57:50.8	M4.5	1.78^b	14.25	11.23	133^e	4	−0.619	−0.346	−34
LHS 3376	18:18:58.7	+66:11:38.2	M4.5	1.70^b	14.16	11.36	137^e	5	0.441	0.440	4
GJ 1227	18:22:27.6	+62:02:35.3	M4.5	1.71^b	13.84	11.01	122^e	2	−0.967	−1.233	−14
LP 229−17	18:34:36.3	+40:07:22.3	M3.5	1.53^b	11.89	9.53	124^e	45	0.046	0.218	12
GJ 1230B	18:41:09.2	+24:47:14.6	M5	1.74^b	14.59	11.68	131^e	9	0.499	0.041	−10
Gl 725A	18:42:46.4	+59:37:51.6	M3	1.39	11.11	9.08	277^f	5	−1.358	1.849	−1
Gl 725B	18:42:47.2	+59:37:37.0	M3.5	1.39	11.92	9.89	277^f	5	−1.358	1.849	1
Gl 745A	19:07:05.7	+20:53:16.0	M1.5	1.23	11.08	9.41	116^f	6	−0.470	−0.336	32
Gl 745B	19:07:13.2	+20:52:36.9	M2	1.23	11.06	9.39	116^f	6	−0.470	−0.336	32
Gl 752A	19:16:55.2	+05:10:07.4	M2.5	1.29	10.24	8.43	168^f	4	−0.593	−1.341	35
GJ 1245AC	19:53:54.2	+44:24:43.6	M5.5	2.01	15.09	11.39	217^e	2	0.418	−0.537	6
GJ 1245B	19:53:55.2	+44:24:43.6	M5.5	2.07	15.69	11.80	217^e	2	0.418	−0.537	5
Gl 791.2	20:29:49.0	+09:41:29.8	M4.5	1.75	13.35	10.42	115^e	2	0.672	0.130	−29
Gl 793	20:30:32.1	+65:26:58.4	M2.5	1.37	10.97	8.99	121^f	2	0.453	0.284	10
Gl 809	20:53:19.9	+62:09:16.1	M0.5	1.07	9.23	7.87	137^f	4	0.010	−0.767	−18
Gl 820B	21:06:55.3	+38:44:31.4	K5	0.80^b	8.36	7.47	293^f	3	4.121	3.130	−65
Gl 829AB	21:29:36.8	+17:38:35.7	M3.5	1.47	11.17	8.95	149^f	5	0.992	0.365	−25
G 188−38	22:01:13.4	+28:18:23.3	M4	1.59	12.26	9.74	112^e	2	0.370	0.051	−3
Gl 849	22:09:40.3	−04:38:27.4	M3.5	1.41	10.54	8.46	108^f	5	1.039	−0.029	−16
Gl 860A	22:27:59.6	+57:41:47.8	M3	1.49	11.82	9.56	248^f	4	−0.853	−0.400	−34
Gl 860B	22:27:59.6	+57:41:47.8	M4	1.49	13.27	11.01	248^f	4	−0.853	−0.400	−35
Gl 873	22:46:49.2	+44:20:00.1	M3.5	1.52	11.73	9.40	197^f	4	−0.701	−0.465	−2
Gl 876	22:53:16.7	−14:15:48.9	M4	1.54	11.74	9.35	206^f	6	0.952	−0.641	−2
Gl 880	22:56:34.8	+16:33:12.2	M1.5	1.11	9.45	8.01	143^f	4	−1.034	−0.287	−28
Gl 896B	23:31:51.7	+19:56:14.2	M4.5	1.62	13.30	10.71	152^e	4	0.559	−0.016	2
GJ 1286	23:35:11.7	−02:23:32.2	M5.5	2.06^b	15.39	11.53	138^e	4	0.774	−0.833	−42
Gl 905	23:41:53.9	+44:09:32.5	M5	1.92	14.79	11.36	316^e	2	0.130	−1.820	−79
GJ 1289	23:43:06.6	+36:32:14.3	M4	1.63^b	13.02	10.40	123^e	3	0.929	−0.145	−3
Gl 908	23:49:12.5	+02:24:05.8	M1	1.08	10.13	8.75	170^f	7	0.997	−0.946	−72

length calibrated spectra, with algorithms described in Baranne et al. (1996). Brighter stars (V<13) were observed with a thorium lamp illuminating the monitoring fiber, as needed for best (15 m.s^{-1}) radial velocity accuracy (Baranne et al. 1996). Fainter stars always have insufficient S/N to reach such an accuracy, and they were instead observed with this fiber illuminated by the sky, allowing subtraction of the diffused solar light whose lines would otherwise bias the velocity profile. Integration times ranged between 10 minutes and 1 hour, and resulted in signal to noise ratios in the 47th order ($\sim$555nm) ranging between 4 and 150, with a median of $\sim$15.

2.3. Rotational velocity analysis

The extracted spectra were analysed for velocity by digital cross-correlation with a binary template (i.e. a spectrum where each pixel is set either to 1 or 0). This processing is standard for ELODIE spectra (Queloz 1995a, 1995b) and it closely mirrors the optical cross-correlation performed in the older CORAVEL spectrograph (Baranne et al. 1979). It effectively amounts to averaging with equal weights the few thousand lines included in the binary template. Given their random blending with weaker lines, and by virtue of the central limit theorem, this results in a very clean, nearly gaussian, instrumental velocity profile. This comes at a price in sensitivity, which could be improved in various ways, for instance by giving more weight to the deeper lines. Useful velocity information can nonetheless still be extracted from spectra with average S/N lower than 1.

The correlation template used for this program was generated by Baranne et al. (1996) from a Bell & Gustafsson (private communication) synthetic spectrum of a K0III star, and is part of the standard ELODIE reduction package. Though not an optimal match for the M stars discussed here, this mask was the reddest available when this program was started, and it generally produces a good correlation dip even for low signal to noise ratio spectra of the later M dwarfs in our sample. As discussed below, the width of this correlation profile for non rotating stars (σ_0) is also nearly constant in the [K7V,M6V] interval. This advantageous feature (for the present purpose) is not shared by the redder masks which have now become available: the intrinsic full width to half maximum of their correlation profile varies by over 1 km.s^{-1} over the [M0V,M6V] range (Delfosse et al. 1997). The calibration of the measured profile width to v sin i is then more difficult, and it would in particular require more accurate $R - I$ colour indexes than are available for a number of stars. The K0 template was thus retained.

The three fastest rotators however produced shallow correlation dips with the K0 mask, since the same equivalent width is then spread over a wider velocity range. This didn't permit an accurate width determination, and they were thus recorrelated with a preliminary M0V mask generated from the observed spectrum of Gl 411 (Queloz, private communication). The resulting correlation dips are twice as deep and the linewidth accuracy correspondingly better. These fast rotators have broad enough lines that the correlation process doesn't measurably widen their correlation dips, and there is no need to calibrate out a contribution of the mask. An equivalent reprocessing was considered unnecessary for slower rotators, since the uncertainty on their v sin i is dominated by the intrinsic dispersion in their unbroadened profile (as discussed below), and improved S/N would not help much. The width of the correlation function was in all cases estimated by fitting a gaussian function. Accurate radial velocities were measured at the same time. They will be used in forthcoming papers to discuss the binary fraction in field M dwarfs and to obtain some accurate stellar masses.

The standard error on the profile width was calibrated as a function of spectral type and signal to noise ratio, through Montecarlo simulations along the lines of Baranne et al. (1996), adding controlled photon noise and CCD readout noise to high signal to noise ratio spectra. Their $C(T_{eff})$ constant (their equation (9)) is 0.085 for early M dwarfs ([M0,M2]) and 0.075 for M3V and cooler spectral types.

2.3.1. v sin i

The resulting profile 1/e half-widths are plotted in Fig. 1a, as a function of the R−I colour index. As can be seen, the plot has a well defined lower envelope, populated by slow rotators and/or nearly pole-on stars, which corresponds to the instrumental profile width σ_0 of the spectrograph+correlation combination. Fig. 1b zooms on this lower envelope and shows a small but significant colour dependence of this instrumental width, better seen in Fig. 1c which only shows the non-active (and thus non-rotating, Sect. 4) stars: σ_0 decreases from $\sim$5.1 km.s^{-1} to $\sim$4.7 km.s^{-1} between R–I=0.8 and R–I=1.5, and seems to saturate for redder stars. A somewhat larger variation is observed for earlier stars, with σ_0 increasing from 4.6 km.s^{-1} to $\sim$ 5 km.s^{-1} over the G0V-K7V spectral range (R–I=[0.3,0.8]), (Queloz 1995a, and private communication). Part of this variation certainly results from the better spectral resolution in the red part of the ELODIE format, which carries increasing weight in the correlation profile for decreasing effective temperatures. Systematic changes in pressure broadening and microturbulent velocity with effective temperature probably contribute too.

At a given R–I colour there is also some significant intrinsic dispersion in σ_0, at a level of $\sim$ ±100 m.s−1 (Fig. 1c). For G and K stars metallicity explains most of this intrinsic dispersion (Queloz, 1995a), with a larger fraction of the lines broadened by saturation in metal-rich stars. The same mechanism must also contribute in M dwarfs, but the Zeeman effect and different levels of microturbulent broadening in individual stars could play a role too.

Given the low level of the σ_0 variations, we have not attempted to calibrate them out. Instead, we have quadratically added a 200 m.s^{-1} systematic uncertainty to the standard errors of all profile width measurements before we determined confidence intervals for v sin i . This currently sets the limit on the accuracy of the measured v sin i : even though ELODIE can measure the 1/e half-width of the correlation profile of bright stars to better than 20 m.s^{-1} (i.e. to 1/200 pixel), we are unable to measure v sin i below $\sim$2 km.s^{-1}.
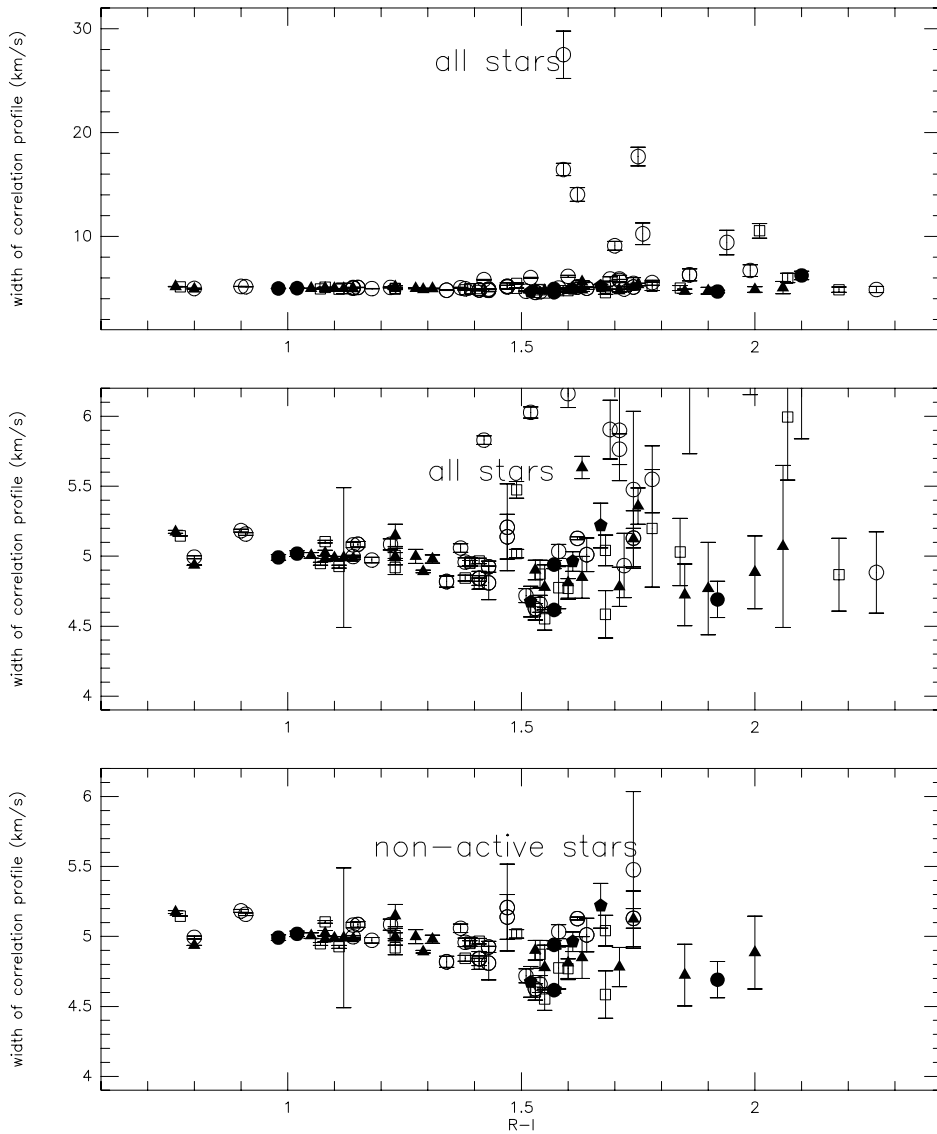
Fig. 1a–c. 1/e half-width of the correlation profile as a function of the $(R - I)_c$ color index for **a** and **b** all stars, and **c** the non-active stars (no H_α emission) only. Symbol codes are: open circles for the young disk, open squares for the young/old disk, filled triangles for the old disk, filled circles for the halo. Known or possible short period binaries (P<30days) have been excluded in these plots.

For warmer stars, the v sin i -σ calibration is established (Queloz 1995a) by convolving the spectrum of a number of stars with known long rotational periods (hence negligible broadening) with a rotational broadening profile (e.g. Gray 1992, p 370), and measuring the resulting correlation width. We use the same method, but there are unfortunately very few rotation period measurements for late main sequence stars: no star later than M2 has a known long rotational period, and for the spectral type range of our sample, only Gl 411 (M2, old disk population, P_{rot} = 48.0days, v sin $i \leq$ 0.4 km.s^{-1}) and Gl 820B (K5, old disk population, P_{rot} = 48.00days, v sin $i \leq$ 0.8 km.s^{-1}) (Hempelmann et al. (1995)) have measured periods that imply v sin $i \lesssim$ 1.5 km.s^{-1}. We have used those two stars for our calibration, and complemented them by Barnard's star (Gl 699, halo M4). Gl 699's rotational period is unknown, but it must be a very slow rotator given its old kinematic population and lack of magnetic activity, and the correlations discussed in Sect. 4. The v sin i difference between the three cal-

ibrations is less than 1 km.s^{-1} below v sin i =8 km.s^{-1}, and only reaches 2 km.s^{-1} at large rotational velocities. The unknown sini factor is then always a more significant uncertainty source in the analysis. We have used the Gl 411 calibration, to which σ = $0.5476 \times \sqrt{v \sin i^2 + 8.467^2}$ is a good analytical fit. 68% confidence intervals for v sin i were obtained by applying the v sin i calibration to ± 1 sigma intervals centered on the measured correlation profile width.

Because rotation and magnetic fields are linked, part or all of the broadening that we attribute to rotation could, in principle at least, be due to Zeeman splitting of individual lines, as first suggested by Benz and Mayor (1984). This would however require rather strong magnetic field, with 3 km.s^{-1} broadening already corresponding to $\sim$5kG (Benz and Mayor, 1984). Such fields have only been found in the most active cool main sequence stars, and appear unlikely for the vast majority of the sample. Zeeman broadening in addition could not explain the faster rotators (v sin $i \gtrsim 10$ km.s^{-1}), since strong magnetic field would
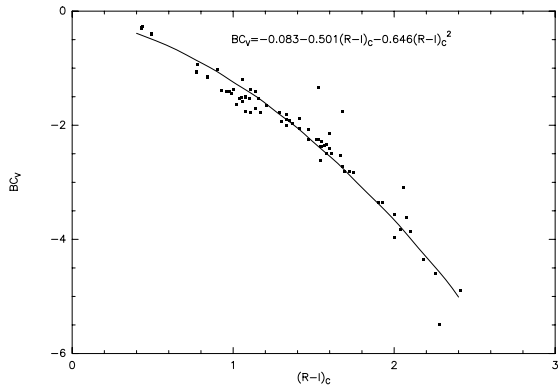
Fig. 2. Bolometric correction curve. The fit is BC_V
$= -0.083 - 0.501(R - I)_C - 0.646(R - I)_C^2$

produce a resolved Zeeman pattern (e.g. Babel et al., 1995) which is quite distinct from the observed rotational profiles. We therefore believe that, with at most a few exceptions, the measured v sin i are indeed due to rotation.

Given the poorer v sin i sensitivity of Stauffer & Hartmann (1986), the most suitable comparison sample is Marcy & Chen (1992), who measured projected rotational velocities for 47 field late-K and M dwarfs, and found measurable rotation (v sin i $> 3 \, \text{km.s}^{-1}$) in only 5. Contrary to them, we find that one quarter of the field M dwarfs have measurable rotation (up to v sin i $\simeq 50 \, \text{km.s}^{-1}$). This apparent discrepancy may be partly due to our slightly lower detection threshold of 2 km.s^{-1}, but it mostly reflects a better sampling of the late M subtypes. As discussed below, the late M dwarfs have a much larger fast rotator fraction. For the 19 stars in common with Marcy & Chen (1992), the two measurements are fully consistent. For Gl 285 and Gl 388 they respectively measure $4.8 \pm 2.3 \, \text{km.s}^{-1}$ and $5.8 \pm 0.5 \, \text{km.s}^{-1}$, where we obtain $6.5 \pm 1.1 \, \text{km.s}^{-1}$ and $6.2 \pm 0.8 \, \text{km.s}^{-1}$. For the 17 other stars their upper limits of $\sim 3 \, \text{km.s}^{-1}$ are consistent with our measurements of at most 2.9 km.s^{-1}. GJ 1111 was measured by Basri & Marcy (1995) and there is also good agreement: they measure $11 \pm 2.5 \, \text{km.s}^{-1}$ where we obtain $8.1 \pm 1.1 \, \text{km.s}^{-1}$.

2.4. L_{H_α}/L_{bol} and L_{H_β}/L_{bol}

A significant fraction of the sample shows emission in the hydrogen Balmer lines, sometimes extending to H_ϵ. We have then used the spectra to determine their H_α and H_β fluxes. We didn't on the other hand attempt measuring the (weaker) Balmer absorption seen in most of the early M spectra.

Since line spectrophotometry wasn't an initial objective of the program, the observations have no matching spectrophotometric calibration. Comparison of two observations of the OV spectro-photometric standard HD93512 separated by $\sim$ one year (D.Queloz, private communication) however shows that the relative efficiency of ELODIE (+telescope+atmosphere) is stable to within $\sim 10\%$ over the [460 nm,680 nm] range, even though variations at bluer wavelength are considerably larger. This interval contains H_α, H_β, and the V filter passband. The

average of these two spectra was thus used to convert all observations to relative flux density.

The calibrated spectra were integrated over the V filter passband and the width of the two Balmer lines to produce relative fluxes in these three bands. Those for the lines were continuum subtracted, using the average flux density of two nearby bandpasses (655.0-655.9 nm and 656.8-657.7 nm for the H_α line; 484.8-485.7 nm and 486.6-487.5 nm for the H_β line) as an estimate of the continuum level at the line wavelength. Continuum definition is difficult for these very cold stars, whose spectra are made up of a forest of overlapping blended lines. For weak chromospheric lines, its uncertainties are the dominant error source on the relative line flux, and they prevent us from measuring equivalent widths smaller than ~ 0.4 Å(typically $L_{H_\alpha}/L_{bol} \simeq 10^{-5}$ for an M5 dwarf). Their contribution to the eventual error bars on L_{H_α}/L_{bol} and L_{H_β}/L_{bol} was estimated from the difference between the continuum computed at the right and at the left of the line, probably giving slightly overestimated errors. The fluxes were then converted to relative luminosities, L_{H_α}/L_V and L_{H_β}/L_V. To convert those to fractional luminosities in the lines, L_{H_α}/L_{bol} and L_{H_β}/L_{bol}, a V band bolometric correction is needed. We have compiled the bolometric correction measurements from Tinney et al. (1993), Berriman & Reid (1987), Reid & Gilmore (1984), and Greenstein (1989), and determined a fit as a function of the $(R–I)_c$ colour: $BC_V = -0.083 - 0.501(R - I)_C - 0.646(R - I)_C^2$ (Fig. 2) $(R–I)_c$ was taken from Leggett (1992) whenever possible, or the Kron R–I listed in the CNS3 catalog (Gliese & Jahreiss 1991) were converted to the Cousin system using the transformation given in Bessel (1983). The resulting Balmer lines luminosities are listed in Table 4.

Standard errors for the fractional luminosities in the two chromospheric lines were estimated from the quadratic sum of the pseudo-continuum definition uncertainty with a 10% uncertainty for the relative spectrophotometric calibration. They are usually much lower than the typical intrinsic variability of the Balmer lines in these active stars: multiple observations of the same star often differ by more than a factor of two.

2.5. L_X/L_{bol}

Schmidt et al. (1995) list the X-ray luminosity of all K and M stars within 7 pc. They have obtained deep ROSAT pointed observations for all their stars which were not detected in the ROSAT all-sky survey (RASS), so the nearer half of our sample has nearly complete X-ray information. Between 7 and 9 pc we have used the RASS catalog data (Voges et al. 1997), with the count-rate to flux calibration (Fleming et al. 1995) used by Schmitt et al. (1995). Use of the RASS data results in a limiting sensitivity of about $2.5 \times 10^{27}[d/10 \, pc]^2 .\text{erg.s}^{-1}$ (Schmidt et al. 1995), and 34 non detections.

2.6. UVW space motion and kinematic population

The UVW space motion in Table 4 is calculated from our measurements of radial velocity, trigonometric parallaxes and

Table 3. Binary stars not considered for the rotation study

Name	α (J2000.0)	δ (J2000.0)	spectral type
LP 476−207	05:01:59.3	+09:58:53.3	M4
Gl 268	07:10:01.8	+38:31:46.4	M4.5
GJ 1103	07:51:55.6	+00:00:50.8	M4.5
GJ 2069A	08:31:37.6	+19:23:39.3	M3.5
GJ 1116	08:58:14.9	+19:45:43.4	M5.5
LHS 6158	08:58:56.0	+08:28:18.8	M3.5
Gl 381	10:12:04.7	−02:41:05.8	M2.5
Gl 473	12:33:17.3	+09:01:16.5	M5
Gl 487	12:49:02.8	+66:06:36.7	M3
LHS 2887	14:17:01.3	+31:42:50.1	M4
Gl 644AB	16:55:28.8	−08:20:11.2	M3
G 203−47	17:09:31.8	+43:40:46.0	M3.5
Gl 661	17:12:07.9	+45:39:59.2	M3.5
Gl 695BC	17:46:25.5	+27:43:00.9	M3.5
GJ 1230A	18:41:09.2	+24:47:08.7	M4.5
Gl 747	19:07:44.7	+32:32:54.5	M3
Gl 831	21:31:18.6	−09:47:25.7	M4.5
Gl 866	22:38:33.8	−15:18:01.6	M5.5
Gl 896A	23:31:52.2	+19:56:15.0	M3.5

proper motions taken from either the Yale General Catalogue of Trigonometric Stellar Parallaxes (Van Altena et al. 1991) or the Hipparcos input catalogue (Turon et al. 1993). U, V and W are heliocentric, with U positive toward the Galactic anticenter. The proper motion standard errors typically translate into ~ 1 km.s^{-1} uncertainties on the space motion, while the parallax typically contribute a $\sim 5\%$ proportional uncertainty. The accurate radial velocities do not contribute appreciably to the overall UVW errors, except perhaps for an occasional unrecognised spectroscopic binary. The space velocities were then used to distribute the stars into young disk, old disk, and Population II, with two intermediate groups young/old disk and old disk/Population II, adopting the criteria of Leggett (1992). Our classification agrees with hers for stars in common, except where our improved radial velocities significantly change the space velocity. It must of course be remembered that these population assignments are only statistically valid, as there is significant overlap between the velocity distributions of the different galactic populations (e.g. Carney et al. 1990). Given the low relative local density of the halo, the older kinematic group is most likely dominated by the thick disk rather than the true halo.

3. Rotational velocities

3.1. Sample pruning

A total of 19 binary stars had to be ignored in the study of the rotational velocity distribution (Table 3). Eight are double-lined spectroscopic binaries with measured or possible short periods: Gl 268 (P=10 days, Tomkin & Pettersen 1986), GJ 1230A (Gizis & Reid 1996), G 203-47, LP 476-207, GJ 2069A (P = 3 days), Gl 896A, LHS 6158 (P = 7.5 days) and LHS 2887 (Delfosse et al. 1997). At short orbital periods (P $\lesssim$ 10 days), rotation is tidally locked to the orbit, and it no

longer reflects the processes at play in an isolated star. Conservatively, we have thus eliminated all binaries whose measured or probable period is less than 30 days.

We have also eliminated 11 multiple systems for which we could not simply disentangle the velocity signatures of the components. Gl 381 is a marginally separated double-lined spectroscopic binary and Gl 487 is a triple-lined system with one long period (Delfosse et al. 1997). The other 9 are known visual or speckle binaries where both stars contribute significant light to the joint spectrum (($\Delta V \leq 2.5$): Gl 473 (Perrier et al. 1991; Henry et al. 1992) Gl 644 (Pettersen et al. 1984), Gl 661 (Henry & McCarthy 1993; Hartkopf et al. 1996)), Gl 695BC (Al-Shukri et al. 1996), Gl 747 (Blazit et al. 1987), Gl 831 (Henry & McCarthy 1993), Gl 866 (Leinert et al. (1990)), GJ 1103AB and GJ 1116AB. Our sample includes a few other speckle binaries (GJ 1245AC, Gl 623, Henry & McCarthy 1993; Gl 234AB, Coppenbarger et al. 1994), but their secondaries are faint enought that they don't affect the rotational velocity measurement of the bright component. Some additional marginally resolved double lined spectroscopic binaries could still remain unrecognised. Over 90% of the sample however now has multiple measurements, separated by typically one year. Since only one such object (Gl 381) has been identified with those data, at most a few should remain in the sample.

Gl 829 and Gl 268.3 are both well separated long period double lined spectroscopic binaries, and each enter as two data points in Table 2. 101 individual measurements therefore contribute to the rotation velocity distribution.

3.2. Distribution of rotational velocities

Fig. 3 shows the distribution of v sin i as a function of the R–I colour index, separately for stars with young and old kinematic characteristics. It is immediately apparent that rotational velocity has a strong dependence on both spectral type (as measured by the R–I color) and dynamic population (used as an ersatz for age). Below $(R–I)_c = 1.4$ (M3V), there is no star with measurable rotation in either plot. Above this value, an increasingly large fraction of the dynamically young stars has large rotational velocities, and beyond $(R–I)_c = 1.9$ (M5.5) essentially all of them rotate. The plot for the older population on the other hand only includes two stars with significant rotation, the M4.5 $((R–I)_c = 1.6)$ dwarf Gl 166C with v sin i = 5.2 km.s^{-1} and the M6 dwarf $((R–I)_c = 2.1)$ Gl 412B with v sin i = 9.4 km.s^{-1}. For the size of the two subsamples ($\sim$ 65 dynamically younger objects and $\sim$ 33 older ones) this difference is statistically significant (Fig. 4).

Given the overlap of the velocity distributions of the various galactic populations, Fig. 3b by necessity contains some younger stars, so that it would in principle be possible that no old star actually has significant rotation. There is indeed good evidence that Gl 166C is a young disk star on the tail of the velocity distribution of its population, since Eggen (1996) deduce an age of only 1.6 Gyr from the Ca$^+$ chromospheric flux of Gl 166A, the K1Ve brightest member of the Gl 166 system (Gl 166B is the prototypical white dwarf 40 Eri B). Based on

Table 4. Rotational, activity and kinematic parameters of the program stars. σ: width of correlation profile with the K0 template, except [a] with the M0 template. The quoted uncertainty on σ is that due to photon and readout noise, while the standard error on v sin i also includes a 200 m.s^{-1} dispersion on σ_0, the width of the correlation profile of a non rotating star. [b]: space velocities were computed using an inaccurate radial velocity (± 2 km.s^{-1}), because we have not yet covered a full orbital period. [c] space velocities use the barycentric radial velocity from Marcy & Chen (1992).

name	σ	err.	v sin i km.s^{-1}	err.	log(L_{BOL}) erg.s^{-1}	log(L_{H_α}) erg.s^{-1}	err.	log(L_{H_β}) erg.s^{-1}	err.	log(L_X) erg.s^{-1}	U	V km.s^{-1}	W	Dyn. Pop.
GJ 1002	4.88	.26	<3.0		30.79	–	–	–	–	<25.55	-37	-41	27	OD
Gl 15A	5.00	.01	<2.9		31.96	–	–	–	–	27.15	49	-12	-3	YD
Gl 15B	5.03	.05	<3.1		31.15	–	–	–	–	26.67	48	-13	-4	YD
Gl 34B	4.99	.01	<2.9		32.37	–	–	–	–	27.15	31	-8	-16	YD
Gl 48	4.84	.02	<2.4		32.18	–	–	–	–	<27.30	64	−39	−14	YO
Gl 49	5.08	.02	<3.4		32.21	–	–	–	–	<27.33	22	−22	4	YD
LP 467-16	9.42	1.18	15.2	2.4	30.99	27.09	.03	26.36	.04	27.80	6	−5	−6	YD
Gl 70	5.00	.04	<3.0		31.72	–	–	–	–	<27.28	−40	−20	2	OD
Gl 83.1	5.36	.13	3.8	1.6	31.05	26.70	.16	26.23	–	27.33	−14	−51	3	OD
Gl 105B	4.81	.12	<2.4		31.58	–	–	–	–	<27.13	79	1	34	OD
Gl 109	4.96	.03	<2.8		31.83	–	–	–	–	27.33	40	−17	−13	YD
GJ 1057	4.72	.22	<2.2		31.11	–	–	–	–	<27.24	60	−42	20	OD
Gl 166C	5.63	.08	5.5	1.3	31.43	27.48	.08	26.74	.02	28.02	−96	−10	−38	OD
Gl 169.1A	4.77	.07	<1.9		31.56	–	–	–	–	26.40	59	−38	−9	YO
LHS 1723	5.04	.11	<3.2		31.31	–	–	–	–	27.35	21	−18	−38	YO
Gl 205	4.99	.01	<2.9		32.44	–	–	–	–	27.57	−25	−59	−11	OD
Gl 213	4.96	.07	<2.9		31.47	–	–	–	–	<26.68	89	−94	9	H
LHS 1805	4.90	.07	<2.7		31.50	–	–	–	–	<27.14	−15	28	10	OD
G 099-049	6.16	.10	7.39	0.8	31.42	27.50	.05	26.98	.01	28.01	26	−16	1	YD
Gl 232	5.01	.12	<3.1		31.15	–	–	–	–	<27.22	−15	−15	7	YD
Gl 234A	5.76	.11	6.0	0.9	31.37	27.32	.06	26.85	–	27.75	3[b]	−24[b]	4[b]	YD
Gl 251	4.84	.02	<2.4		31.84	–	–	–	–	26.01	28	−3	−17	YD
LHS 1885	5.03	.24	<3.7		31.08	26.90	.07	26.35	.05	28.30	17	−10	15	YO
GJ 1093	4.77	.33	<2.8		30.67	25.82	.66			<27.16	−43	−33	10	OD
Gl 268.3A	4.92	.04	<2.7		31.79	–	–	–	–	<27.18	−6	−8	−7	YD
Gl 268.3B	4.81	.12	<2.4		31.79	–	–	–	–	<27.18	−6	−8	−7	YD
Gl 273	4.78	.16	<2.4		31.65	–	–	–	–	25.88	−16	−65	−17	OD
G 089−032	6.30	.57	7.9	2.1	31.07	27.08	.08	26.01	.15	<26.96	13	−23	8	YD
Gl 285	5.91	.21	6.5	1.1	31.69	28.03	.02	27.44	.02	28.67	20	−22	−10	YD
GJ 1105	4.63	.08	<2.0		31.45	–	–	–	–	<27.21	−19	−28	−8	YD
Gl 299	5.22	.16	3.0	1.7	31.10	–	–	–	–	<25.55	−71	−155	−31	H
GJ 2066	4.92	.05	<2.7		32.00	–	–	–	–	<27.27	54	−34	7	YO
GJ 1111	4.88[a]	.29	8.1	1.1	30.48	26.09	.05	25.26	.23	26.60	17	−10	−13	YD
GJ 2069B	5.90	.36	6.5	1.7	31.17	27.28	.03	26.70	.04	28.40	8	−5	−8	YD
Gl 338A	5.18	.01	2.9	1.2	32.44	–	–	–	–	27.51	42	−16	−24	YD
Gl 338B	5.16	.01	2.8	1.2	32.41	–	–	–	–	27.51	43	−15	−23	YD
Gl 380	5.14	.01	2.8	1.4	32.49	–	–	–	–	27.45	7	−19	−35	YO
Gl 382	4.97	.02	<2.9		32.27	–	–	–	–	27.44	3	−13	−3	YD
Gl 388	5.83	.03	6.2	0.8	31.94	28.17	.03	27.68	.02	28.92	15	−7	3	YD
Gl 393	5.00	.02	<2.9		32.08	–	–	–	–	<27.17	7	−30	−18	YO
Gl 402	4.78	.15	<2.3		31.54	–	–	–	–	<26.82	11	−29	−24	YO
Gl 406	4.87	.26	<2.9		30.55	26.44	.04	25.46	.08	27.78	27	−45	−16	YO
Gl 408	4.82	.04	<2.3		31.89	–	–	–	–	<27.04	9	−11	−4	YD
Gl 411	4.99	.01	<2.9		31.90	–	–	–	–	26.84	−46	−54	−75	OD
Gl 412A	5.02	.02	<3.0		32.01	–	–	–	–	<26.00	141	−7	7	HO
Gl 412B	6.25	.41	7.7	1.7	30.84	26.79	.08	26.35	.03	27.56	141	−7	7	HO
Gl 424	5.00	.02	<2.9		32.09	–	–	–	–	<27.24	133	−8	0	HO
Gl 445	4.67	.11	<2.0		31.51	–	–	–	–	26.63	−46	11	−104	H
Gl 447	4.58	.17	<2.0		31.18	–	–	–	–	26.78	−18	6	−33	YO
GJ 1151	5.12	.20	<4.1		31.18	–	–	–	–	<27.21	27	−66	−34	OD
Gl 450	5.08	.02	<3.3		32.12	–	–	–	–	27.71	16	5	−5	YD
LHS 2520	4.62	.02	<2.0		31.54	–	–	–	–	<27.28	−29	−71	37	HO

Table 4. (continued)

name	σ	err.	$v\sin i$ (km.s^{-1})	err.	$\log(L_{BOL})$ erg.s^{-1}	$\log(L_{H_\alpha})$ erg.s^{-1}	err.	$\log(L_{H_\beta})$ erg.s^{-1}	err.	$\log(L_X)$ erg.s^{-1}	U	V (km.s^{-1})	W	Dyn. Pop.
GJ 1154A	5.55	.24	5.2	2.1	31.05	27.19	.05	26.60	.01	27.77	28	-20	-22	YD
GJ 1156	6.71	.56	9.2	1.9	31.04	27.06	.04	26.65	.01	27.65	37	-14	1	YD
Gl 486	4.55	.08	<2.0		31.83	$-$	$-$	$-$	$-$	<27.32	24	-43	11	YO
Gl 493.1	10.25	1.04	16.8	2.1	31.13	27.17	.05	26.67	.06	27.92	40	-5	-21	YD
GJ 2097	5.13	.07	<3.7		31.23	$-$	$-$	$-$	$-$	<26.69	2	-1	-11	YD
Gl 514	5.01	.02	<2.9		32.22	$-$	$-$	$-$	$-$	27.47	-61	-9	-5	OD
G 165-08	27.51^a	2.28	55.5	8.4	31.50	27.89	.01	27.43	.01	28.31	4	-8	10	YD
Gl 526	4.98	.02	<2.9		32.04	$-$	$-$	$-$	$-$	26.60	-57	-2	-2	OD
Gl 555	5.13	.01	2.7	1.6	31.63	$-$	$-$	$-$	$-$	<26.67	15	7	14	YD
Gl 581	4.80	.04	<2.1		31.74	$-$	$-$	$-$	$-$	<26.44	23	-31	9	YO
Gl 623	4.98	.03	<2.9		31.87	$-$	$-$	$-$	$-$	<27.14	-22^c	2^c	-47^c	YO
Gl 625	5.08	.04	<3.4		31.73	$-$	$-$	$-$	$-$	26.88	-7	-2	-19	YD
Gl 628	4.72	.05	<1.1		31.60	$-$	$-$	$-$	$-$	26.44	13	-19	-21	YD
Gl 643	4.87	.10	<2.7		31.28	$-$	$-$	$-$	$-$	26.76	-19	-31	10	YO
Gl 673	5.17	.01	2.8	1.1	32.60	$-$	$-$	$-$	$-$	27.64	-1	-54	-10	OD
Gl 686	4.99	.50	<5.0		31.99	$-$	$-$	$-$	$-$	<27.15	32	33	-20	OD
Gl 687	4.97	.02	<2.8		32.02	$-$	$-$	$-$	$-$	26.88	-33	-26	-7	YO
Gl 699	4.94	.03	<2.8		31.17	$-$	$-$	$-$	$-$	25.58	141	4	19	HO
Gl 701	5.10	.01	<3.5		32.03	$-$	$-$	$-$	$-$	<27.13	-32	14	-18	YO
GJ 1224	5.20	.42	<5.6		30.99	26.96	.07	26.32	.03	27.93	28	-29	12	YO
LHS 3376	9.10	.43	14.6	1.0	30.94	26.86	.09	26.26	.10	27.31	17	8	-10	YD
GJ 1227	4.78	.14	<2.3		31.07	$-$	$-$	$-$	$-$	<27.21	-53	-25	21	OD
LP 229-17	4.60	.06	<2.0		31.67	$-$	$-$	$-$	$-$	<27.19	4	13	5	YO
GJ 1230B	5.48	.56	<7.1		30.81	$-$	$-$	$-$	$-$	27.66	10	1	-18	YD
Gl 725A	4.95	.02	<2.8		31.85	$-$	$-$	$-$	$-$	26.30	26	-13	27	YO
Gl 725B	4.96	.03	<2.8		31.52	$-$	$-$	$-$	$-$	26.30	26	-11	28	YO
Gl 745A	5.00	.06	<3.0		31.72	$-$	$-$	$-$	$-$	<27.25	-35	12	14	OD
Gl 745B	5.15	.08	2.8	1.6	31.73	$-$	$-$	$-$	$-$	<27.25	-35	12	14	OD
Gl 752A	4.89	.01	<2.6		32.11	$-$	$-$	$-$	$-$	26.71	-53	-9	-5	OD
GJ 1245AC	10.55	.70	17.4	1.4	30.92	26.65	.09	25.99	.04	27.18	-7	6	-13	YO
GJ 1245B	6.00	.45	6.8	1.9	30.76	26.51	.10	25.85	.03	27.18	-7	6	-13	YO
Gl 791.2	17.70^a	.90	32.0	2.0	31.31	27.30	.06	26.82	.02	27.88	36	-16	-11	YD
Gl 793	5.06	.03	<3.2		31.88	$-$	$-$	$-$	$-$	27.80	21	9	-6	YD
Gl 809	4.95	.01	<2.8		32.33	$-$	$-$	$-$	$-$	27.47	-22	-11	-20	YO
Gl 820B	4.94	.01	<2.8		32.49	$-$	$-$	$-$	$-$	27.02	90	-54	-9	OD
Gl 829A	5.14	.16	<4.0		31.90	$-$	$-$	$-$	$-$	<26.86	38	-17	-4	YD
Gl 829B	5.21	.31	<5.3		31.90	$-$	$-$	$-$	$-$	<26.86	38	-17	-4	YD
G 188-38	16.45^a	.60	29.4	1.2	31.58	27.85	.03	27.43	.02	28.44	14	-4	-7	YD
Gl 849	4.84	.05	<2.4		32.09	$-$	$-$	$-$	$-$	<27.31	42	-18	-16	YD
Gl 860A	5.02	.03	<3.0		31.66	$-$	$-$	$-$	$-$	27.38	-26	-28	2	YO
Gl 860B	5.47	.06	4.7	1.5	31.08	26.97	.11	26.52	.04	27.38	-26	-28	2	YO
Gl 873	6.03	.04	6.9	0.8	31.72	28.02	.03	27.62	.01	29.08	-20	1	-1	YD
Gl 876	4.66	.06	<2.0		31.74	$-$	$-$	$-$	$-$	26.51	13	-20	-11	YD
Gl 880	4.92	.01	<2.8		32.28	$-$	$-$	$-$	$-$	27.17	-33	-17	25	YO
Gl 896B	14.04	.66	24.2	1.4	31.20	27.36	.05	26.88	.02	28.62	15	-5	-7	YD
GJ 1286	5.07	.58	<5.7		30.87	25.91	.61	25.05	6.63	<27.10	12	-54	16	OD
Gl 905	4.69	.13	<1.2		30.94	$-$	$-$	$-$	$-$	27.19	-34	-76	-3	HO
GJ 1289	4.85	.15	<2.6		31.32	$-$	$-$	$-$	$-$	27.70	28	-19	-13	OD
Gl 908	5.02	.02	<3.0		31.98	$-$	$-$	$-$	$-$	27.10	9	-70	40	OD
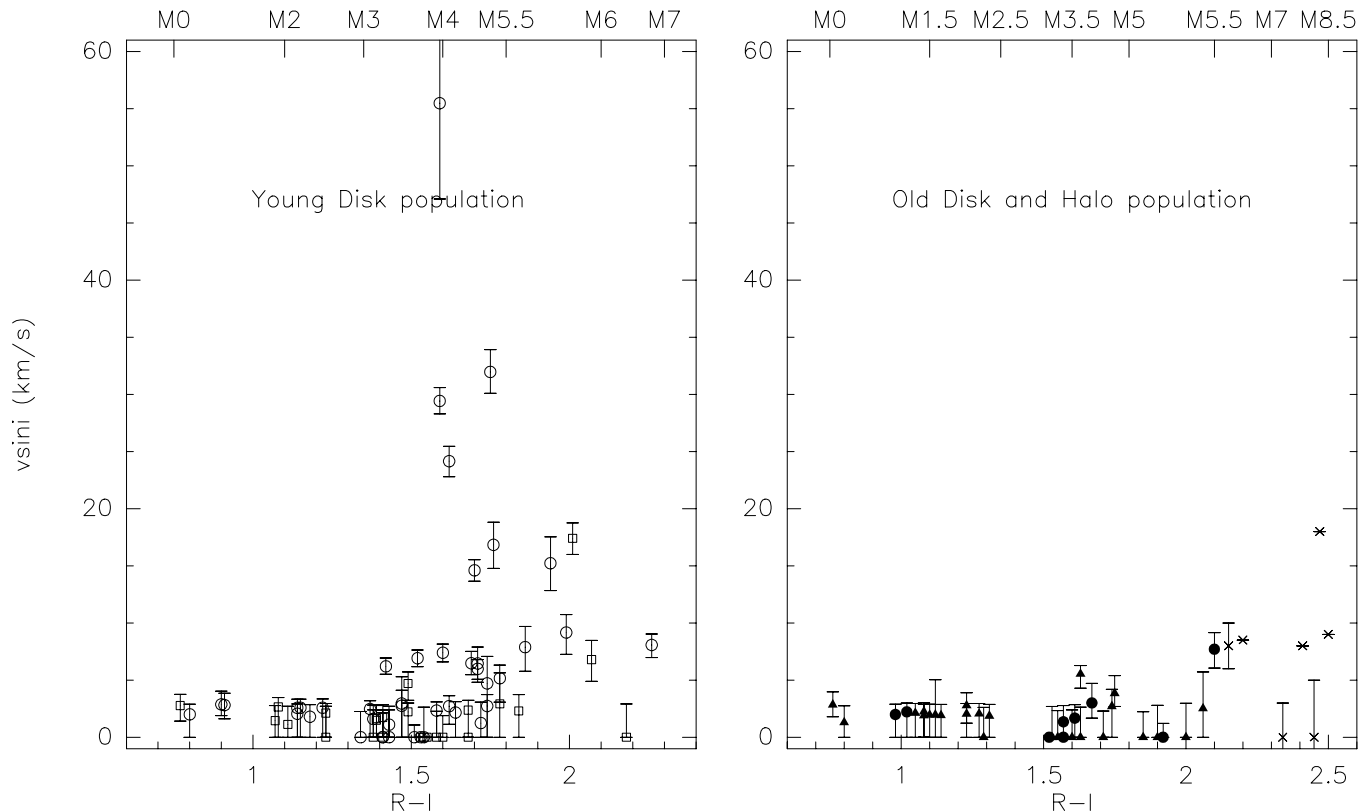
Fig. 3a and b. Projected rotational velocity as a function of the $(R–I)_c$ color index for **a** stars with young disk kinematics, and **b** stars with kinematics typical of older populations. Known short period binaries or binaries with blended correlation profile have been excluded in both plots. The symbol coding is the same as in Fig. 1, except that stars in b) are old disk stars from Basri et al. 1996.

the same argument for Gl 412A, the Gl 412 system on the other hand is 9 Gyr old (Eggen 1996), and Gl 412B is thus probably a true member of the old disk, with significant rotation. At spectral type M6V it is also one of the latest star in the sample, consistent with a general increase of spin-down timescale with decreasing mass, which we advocate for below. This is in line with recent measurements by Basri et al. (1996) who find significant rotation (v sin i >5 km.s^{-1}) for 13 out of 18 very late M dwarfs (>M6.5V). Some of them have no published radial velocities, but there are at least 7 which kinematically belong to the old disk population.

Adopting the calibration of Kirkpatrick & McCarthy (1994), the mass at the M3-M4 spectral type of the break in the rotational velocity distribution of the young population is 0.18 to 0.25M$_\odot$. This break could thus possibly correspond to the mass (0.35±0.05M$_\odot$, Chabrier & Baraffe 1997) below which main sequence stars become fully convective. The radiative/convective boundary is essential to the operation of the shell dynamo which is invoked to explain the large scale solar magnetic field (e.g. Spiegel & Weiss 1980; Spruit & van Ballegooijen 1982), and a change at about this spectral type could thus be expected for both magnetic properties and rotational braking. This approximate agreement must however be coincidental, since a similar feature should otherwise be present at this spectral type in the rotational velocity distribution of the old

stellar population, and none is seen. In addition, the recent mass to spectral type calibration of Baraffe & Chabrier (1996) pushes the full convection limit to earlier than M2.5, inconsistent with the position of the break. We therefore believe that, instead of a break at 0.35M$_\odot$, we observe the continuation to lower masses of the increase in spin-down timescale with decreasing mass, seen in young clusters for the more massive star. This implies that the spin-down timescale is a significant fraction of the age of the young disk (~3 Gyr: Mayor 1974; Meusinger et al. 1991) at spectral type M4 (~0.15M$_\odot$, Baraffe & Chabrier 1996), and a significant fraction of the age of the old disk (~10 Gyr) at spectral type M6 (~0.1M$_\odot$).

3.3. Fast rotators

In our sample seven stars have v sin $i \geq$ 15 km.s^{-1} and three are fast rotators, with v sin $i \geq$ 30 km.s^{-1}: the M4 dwarfs G165-08 (v sin i = 51.5 ± 4 km.s^{-1}), and G188-38 (v sin i = 29.6 ± 1.2 km.s^{-1}) and the M4.5 dwarf Gl 791.2 (v sin i = 32.1 ± 1.7 km.s^{-1}). Adopting radii of respectively 0.3R$_\odot$ and 0.2R$_\odot$ for M4V and M4.5V (Chabrier & Baraffe 1995), the maximum rotational periods P/sini for these three stars are respectively 7.2, 12.7 and 8 hours. For a more massive G dwarf, the same periods would correspond to rotational velocities of v sin i of 170-100 km.s^{-1}, similar to those of the fastest rotators in young

open clusters. With a large telescope, these three stars would be good candidates for a doppler imaging program, and could provide extremely important constraints on the magnetic field geometry in fully convective stars.

4. Rotation versus activity

The relation between magnetic activity and rotation is observationally well established for G and K dwarfs (e.g. Soderblom et al. 1993 and Stauffer et al. 1994 for recent reviews of the connection with respectively chromospheric and coronal activity), and for M dwarfs in young clusters (e.g. Stauffer et al. 1997). Rotation drives the shell dynamos which are believed to excite stellar activity, and faster rotation excites stronger magnetic activity, up to a saturation threshold of ~ 10 km.s^{-1}. We show here that similar relations hold for the field M dwarfs and observe no break in these relation at the spectral type where the stars become fully convective, and where shell dynamos must stop working.

4.1. Chromospheric activity

Fig. 5 shows the fractional luminosity in the first two Balmer lines as a function of v sin i , and indicates a saturation type relation between these chromospheric activity diagnostics and the rotational velocity. All stars with a significant v sin i have chromospheric activity as well, and the two flux ratios saturate for rather low velocities, of the order of our detection limit of 2 km.s^{-1}. Most of the slowly rotating stars only have upper limits for both v sin i and the Balmer line luminosities, so that we are unable to document the chromospheric activity increase with rotation velocity, which presumably occurs at lower v sin i . The saturation levels ($L_{H_\alpha}/L_{bol})\sim 10^{-3.5} - 10^{-4}$, and $L_{H_\beta}/L_{bol}\sim 10^{-4} - 10^{-4.5}$) are similar to those observed for earlier M dwarfs in the Hyades and Pleiades (Reid et al. 1995b; Stauffer et al. 1997).

The fraction of magnetically active stars amongst field M dwarfs has long been known to depend on both spectral type and age, as probed by the dynamical population (Stauffer & Hartmann 1986). Field M dwarfs with Balmer line emission become more frequent at later M types, and they represent a dynamically younger population than the non-active stars. The present data show that rotation is the underlying physical parameter and that the longer spin-down timescale at lower masses explain both behaviours.

4.2. Coronal activity

X-ray emission is the most convenient indicator of coronal activity, and for younger and more luminous stars is well known to correlate with stellar rotation (Bouvier 1990; Fleming et al. 1989). For the Pleiades G, K and M dwarfs for instance, Stauffer et al. (1994) find that L_X/L_{bol} rises rapidly with rotational velocity until v sin i ~ 15 km.s^{-1}, and then remains approximately flat at $L_X/L_{bol}\sim 10^{-3}$.
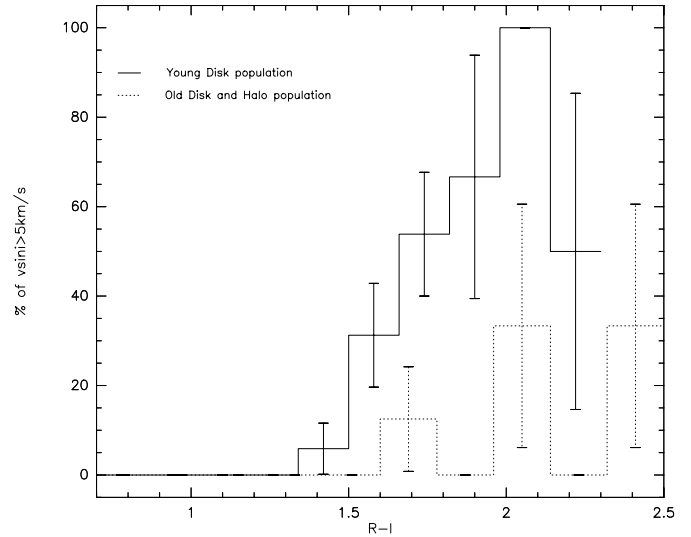
Fig. 4. Fraction of stars with large rotational velocity (v sin i >5 km.s^{-1}) as a function of their spectral type.

Fig. 5 displays the same diagram for the present sample of field M dwarfs, and indicates a qualitatively similar saturation behaviour. Saturation occurs at $\log(L_X/L_{bol})\sim -3$, the value found for M dwarfs in the Pleiades (Stauffer et al. 1994) and the Hyades (Reid et al. 1995b; Stauffer et al. 1997). The saturation velocity, on the other hand, is a factor of 3 lower than for the cluster M dwarfs, at v sin i $\sim 4 - 5$ km.s^{-1} instead of v sin i ~ 15 km.s^{-1}. The poorer spectral resolution of the cluster data and the smaller fraction of open cluster M dwarfs with x-ray data may contribute to a larger apparent saturation velocity: the rising part of the relation is not very well documented, and (in both cases) occurs close to the the minimum measurable rotational velocity. The most likely explanation for most of this difference is however the typically larger stellar radius in the cluster samples, since the rotation rate Ω (or more precisely the Rossby number) is expected to be the relevant parameter, rather than the equatorial velocity (e.g. Barnes & Sofia, 1996; or Krishnamurthi et al. 1997). The cluster samples are biased towards early M types, while the effective spectral type interval in Fig. 5 is $\sim$ [M4,M6]: since no field star earlier than M3.5 has measurable rotation, the relation between coronal activity and rotation is only defined by cooler stars. Adopting representative spectral types of M2V for the cluster samples and M5V for the rotating nearby stars, typical radii are thus respectively $\sim 0.45 R_\odot$ and $\sim 0.15 R_\odot$ (Chabrier & Baraffe, 1995), and the two saturation velocities correspond to a similar rotational period of P~ 1.5 day. Within our sample, there are possible indications for a spectral type dependence of the saturation velocity, though their significance is marginal. The apparent effect could still result from small number statistics, or be an artefact of our imperfect calibration of the instrumental correlation profile as a function of spectral type.
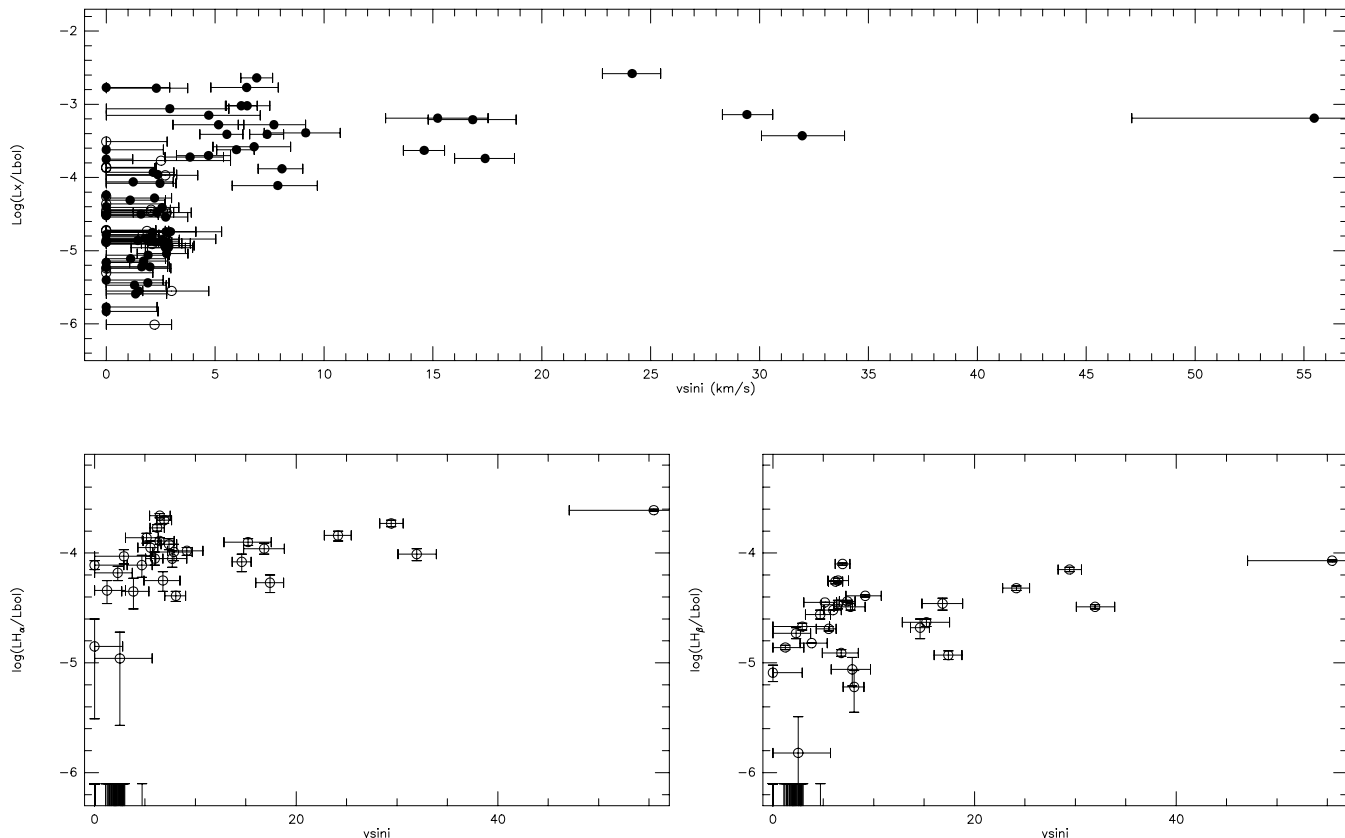
Fig. 5. Chromospheric and coronal activity diagnostics as a function of the projected equatorial velocity

4.3. Activity in fully convective stars

The extreme M dwarf BRI 0021+0214 (M9.5+, v sin i =40±7 km.s^{-1}, Basri & Marcy 1995), on the other hand, has fast rotation and extremely faint Hα emission (Basri & Marcy 1995), though it is detectable (Tinney et al. 1997). As this is clearly at odds with what is seen in young early M dwarfs (e.g. Stauffer et al. 1997; Stauffer et al. 1994; Patten & Simon 1996), and since the behaviour of mid-M dwarfs was then unknown, Basri & Marcy (1995) tentatively attributed this behaviour to a change in the dynamo processus at the mass (0.35 M$_{\odot}$ (Chabrier & Baraffe 1997), corresponding to M2.5V (Baraffe & Chabrier 1996)) where stars become fully convective.

The present data show no obvious feature in the rotational velocity distribution at this spectral type, or elsewhere within the M0-M6 range. The activity/rotation relation for the fully convective M3-M6 dwarfs is also similar to that for young more massive stars that retain a radiative core. The change in this relation seen for M9.5V stars ($\lesssim 0.08 M_{\odot}$) must therefore happen at a spectral type later than M6V (0.1M$_{\odot}$), and is thus not directly related to the transition to full convection. Since the radiative/convective boundary is essential to the operation of the standard $\alpha - \Omega$ dynamo responsible for the large scale solar magnetic field, a different mechanism has to be invoked to explain the observed magnetic activity in low mass stars, as discussed by Durney et al. (1993). They show that a small scale, turbulent,

magnetic field can be generated even in fully convective stars and is mildly enhanced by rotation. The source of stellar magnetic activity should therefore change from the large scale field in solar mass stars to a turbulent field in the fully convective low mass stars. The lack of a sharp boundary at the fully convective mass limit shows that the turbulent field already drives most of the magnetic activity in stars which retain a significant radiative core.

5. Summary and conclusions

We have derived rotational velocities for a volume limited sample of field M0-M6 dwarfs. We find no measurable rotation in the M0-M3 range. Later than M4 ∼ 25% of the young disk field stars are rapid rotators. We identify a single old disk star with significant rotation, at spectral type M6. Complementing our data with published rotational velocities shows that at this spectral type rotation becomes common-place in the old kinematic populations (old disk and population II) . These new data extend to lower masses and older ages the well known increase of the spin-down timescale for decreasing masses: measurable rotation is found in G dwarfs at the age of α Per (50 Myr), in K dwarfs at the age of the Pleiades (70 Myr), and early M dwarfs in the Hyades (500 Myr). We show that the spin-down timescale is of the order of a few Gyr at spectral type M3-M4, and of the order of 10 Gyr at spectral type M6.

We also show that the well established saturated correlations between rotation and magnetic activity in earlier or younger stars continue in the late field M dwarfs. Saturation occurs for lower rotational velocities but similar rotational periods, roughly consistently with expectations if the Rossby number controls magnetic activity. We find no earlier type equivalent of the fast rotating very late M dwarfs with no measurable chromospheric emission in the Balmer lines. This unexplained phenomenon is therefore only found at spectral types later than M7V.

The present data also imply that rotation is the underlying variable which explains why later type and kinematically younger M dwarfs are more likely to display Hα emission, as more massive or older stars have had time to spin down to low rotation rates which no longer generate detectable chromospheric emission in the Balmer lines.

Neither the rotational velocity distribution nor the rotation/activity relation show marked features at the spectral type where stars become fully convective. This implies that the transition from a solar-like shell dynamo to magnetic activity driven by another dynamo type (probably turbulent) must occur in stars that retain a sizeable radiative core.

Future work should include rotational period determinations for field M dwarfs, which can be obtained on modest-size telescopes. Since they are free of the orientation uncertainty inherent to v sin i , and can probe much slower rotation, they would define the low mass rotation/activity relations with much reduced observational scatter in the saturated range and confirm it in the unsaturated domain. v sin i measurements for a significantly larger sample would also be very useful, and would better establish the characteristics of the rotation onset at spectral type M3/M4 in the young disk and spectral type M6 in old populations. Finally, Doppler imaging of the fast rotators we have identified can be performed with a 10m-class telescope and would determine the spatial distribution of magnetic activity on the surface of fully convective low mass stars. This crucial information is probably the most direct probe of their magnetic field geometry and would provide a much needed constraint on the mechanism of their dynamo. The generally advocated turbulent field dynamos (Durney et al. 1993, Weiss 1993) probably imply a spatially uniform chromospheric activity, and this is easily tested by a single Doppler image. They would also not sustain cycles analogous to the solar cycle, and at least in principle this can be tested through Doppler imaging monitoring.

References

Al-Shukri A. M., McAlister H. A., Hartkopf W. I., Hutter D. J., Franz O. G., 1996, AJ 111, 393.

Babel J., North P., Queloz D., 1995, A&A 303, L5.

Baraffe I., Chabrier G., 1996, ApJ 461, L51.

Baranne A., Mayor M., Poncet J.L. 1979, Vistas in Astronomy 23, 279.

Baranne A., Queloz D., Mayor M. et al., 1996 A&AS 119, 373.

Barnes S., Sofia S., 1996 ApJ 462, 746.

Basri G., Marcy G. W., 1995, AJ 762, 109.

Basri G., Marcy G. W., Oppenheiler B., Kulkarni S., Nakajima T., 1996, in Pallavicini and Dupree (eds) 9th Cambridge Workshop, ASP Conf. Series vol. 109, p. 587.

Blazit A., Bonneau D., Foy R., 1987, A&ASS 71, 57.

Benz W., Mayor M., 1984, A&A 138, 183.

Berriman G., Reid I. N., 1987, MNRAS 227, 315.

Bessel M. S., 1983, PASP 95, 480.

Bessel M. S., 1990, A&ASS 83, 357.

Bouvier J., 1990, AJ 99, 946.

Bouvier J., Cabrit S., Fernandez M., Martin E. L., Matthews J. M., 1993, A&A 272, 176.

Bouvier J., Forestini M., 1995, in: "Circumstellar Dust Disks and Planet Formation", ed. R. Ferlet.

Bouvier J., Wichmann K., Grankin K. et al., 1997 A&A in press

Cameron A.C., Campbell C.G., 1993, A&A 274, 309.

Carney B. W., Latham D. W., Laird J. B., 1990, AJ 99, 572.

Chabrier G., Baraffe I., 1995, ApJ 451, L29.

Chabrier G., Baraffe I., 1997, A&A in press.

Chabrier G., Baraffe I., Plez B., 1996, ApJ 459, L91.

Coppenbarger D. S., Henry T. J., McCarthy Jr D. W., 1994, AJ 107, 1551.

Delfosse X., Forveille T., Udry S., Beuzit J. L., Mayor M., Perrier C., 1997, in preparation for A&A.

Durney B. R., De Young D. S., Roxburgh I. W., 1993, SoPh 145, 207.

Eggen O. J., 1996, AJ 111, 466.

Fleming T. A., Molendi S., Maccacaro T., Wolter A., 1995, ApJSS 99, 701.

Gizis J. E., Reid I. N., 1996, AJ 111, 365.

Gliese W., Jahreiss H., 1991, Preliminary Version of the Third Catalogue of Nearby Stars, as available at CDS Strasbourg.

Greenstein J. L., 1989, PASP 101, 787.

Gray D. F., 1992, "The observation ans analysis of stellar photospheres", second edition, Cambridge University Press.

Hartkopf W. I., Mason B. D., McAlister H. A., 1996, AJ 111, 370.

Hempelmann A., Schmitt J. H. M. M., Schultz M., Rudiger G., Stepien K., 1995, A&A 294, 515.

Henry T. J., Johnson D. S., McCarthy Jr D. W., Kirkpatrick J. D,. 1992, A&A 254, 116.

Henry T. J., McCarthy Jr D. W., 1993, AJ 106, 773.

Henry T. J., Kirkpatrick J. D, Simons D. A., 1994, AJ 108, 1437.

Jones B. F., Fischer D. A., Stauffer J. R., 1996, AJ 112, 1562.

Kirkpatrick J. D., McCarthy D. W., 1994, AJ 107, 333.

Krishnamurthi A., Pinsonneault M. H., Barnes S., Sofia S., 1997, ApJ in press.

Leggett S. K., 1992, ApJS 82, 351.

Leinert C., Haas M., Allard F., Wehrse R., McCarthy Jr D. W., Jahreiss H., Perrier C., 1990, A&A 236, 399.

Marcy G. W., Chen G. H., 1992, ApJ 390, 550.

Martin E. L., Claret A., 1996, A&A 306, 408.

Martin E. L., Zapatero Osorio M. R., Rebolo R., 1996, in Pallavicini and Dupree (eds), 9th Cambridge Workshop, ASP Conf. Series vol. 109, p. 615.

Mayor M., 1974, A&A 32, 321.

Meusinger H., Reiman H. G., Stecklum B., 1991, A&A 245, 57.

Patten B.M., Simon T., 1996, ApJSup 106, 489.

Perrier C., Mariotti J. M., Bonneau D., Duquennoy A., (1991), in Beckers J.M. & Merckle F. (Eds), Proceedings of the second ESO-NOAO conference on high angular resolution, ESO, Garching bei München, Germany.

Pettersen B. R., Evans D. S., Coleman L. A., 1984, ApJ 282, 214.

Prosser C. F., 1991, Ph.D. Dissertation, Univ. Calif. Santa Cruz.

Queloz D. 1995a, PhD Thesis 2788, University of Geneva

Queloz D. 1995b, in IAU Symposium 167, "New developments in array technology and applications", ed. A.G. Davis Philip (Dordrecht: Kluwer), 221.

Reid I. N., Gilmore G, 1984, MNRAS 206, 19.

Reid I. N., Hawley S. L., Gizis J. E., 1995a, AJ 110, 1838.

Reid I. N., Hawley S. L., Mateo M., 1995b, MNRAS 272, 828.

Schatzman E., 1962, Ann. d'Ap. 25, 18.

Schmidt J. H. M. M., Fleming T. A., Giampapa M. S., 1995, ApJ 450, 392.

Shu F., Najita J., Ostriker E., Wilkin F., Ruden S., Lizano S. 1994, ApJ 429, 781.

Skumanich A., 1972, ApJ 171, 565.

Soderblom D. R., Stauffer J. R., Hudon D., Jones H., 1993, ApJS 85, 315.

Spiegel E. A., Weiss N. O., 1980, Nature 287, 616.

Spruit H. C., van Ballegooijen A. A., 1982, A&A 106, 58.

Stauffer J. R., Hartmann L. W., 1986, ApJS 61, 531.

Stauffer J. R., Hartmann L. W., 1987, ApJ 318, 337.

Stauffer J. R., Hartmann L. W., Latham D. W., 1987, ApJ 320, L51.

Stauffer J. R., Caillault J. P., Gagné M., Prosser C. F., Hartmann L. W., 1994, ApJS 91, 625.

Stauffer J. R., Balachandran S. C., Krishnamurthi A. et al., 1997, ApJ 475, 604.

Tomkin J., Pettersen B. R., 1986, AJ 92, 1424

Tinney C. G., Mould J. R., Reid I. N., 1993 AJ 105, 1045.

Tinney C. G., Delfosse X., Forveille T., 1997, submitted to ApJ Letters.

Turon C., et al, 1993, Hipparcos Input catalogue, version 2, Bull Inf Centre Donnees Stellaires, 43, 5.

Van Altena W.F., Lee J.T., Hoffleit D., 1991, The General Catalogue of Trigonometric Stellar Parallaxes, Preliminary Version, Yale University Observatory (1991).

W. Voges, B. Aschenbach, Th. Boller, et al., 1997, to be published in A&A.

Weiss, N.O., 1993, in Physics of Solar and Stellar Coronae, Linsky J.F. and Serio S. (eds.), Kluwer (Dordrecht).